On the Use of Vibration Synthesis to ease Electric Machine Powertrain Design

Chauvicourt F., Ciceo S., Van der Auweraer H.
Engineering Services RTD
Siemens Industry Software NV
Leuven, Belgium
fabien.chauvicourt@siemens.com

***Abstract*—This paper provides e-machine designers a critical study on the vibration synthesis algorithm that calculates the vibrations of an electric machine responsible for magnetic noise. It separates the computations into two distinct categories: offline and online. Comprehensive parameters are input to an offline simulation system where generic magnetic forces and vibration transfer functions are created. This generic data combined with operational loads from system-level simulations refers to the online simulation environment. The methodology is applied to an interior Permanent Magnet Synchronous Machine (PMSM), and compared to the standard procedure where run-up simulation can become time-expensive due to the extensive use of Finite Elements (FE) methods. Vibration results show discrepancies of harmonic amplitude content essentially coming from the force truncation made in the vibration synthesis, for which a selection protocol is proposed. Yet the offline simulations permit to front-load the computational efforts thus implying the use of the technique in system-simulation environments.**

***Index Terms*—vibration synthesis, electric machine, simulation, PMSM, computational effort**

I. Introduction

With the growing expansion of electric vehicles and the need for efficient system-level designing processes, it is essential to define simulation frameworks that comply with accuracy, speed while incorporating every important physics of the system. For electric machine powertrains, not only the overall efficiency but also the Noise and Vibration (NV) characteristics are gradually introduced in the design optimization schemes, essentially with the emerging technologies relying less on permanent magnets [1]. The particular whining noise associated to electric machines eventually disturbs comfort and originates from a chain of multiple physical phenomena. Electromagnetic field variations generate magnetic forces in the air-gap which apply on both the stator and the rotor. In the case of outer stator topology, the forces activate the stator in the form of vibrations that latter translate to acoustic pressure fluctuations through structural surface velocity [2].

In practice, this phenomenon can be simulated fully analytically. Eventually equivalent circuits of the machine permit to compute airgap forces which are input of a simple structural ring model, and where acoustic pressure is estimated from finite/infinite cylinder theory [3]. Although impressively fast, this method lacks accuracy. Finite Element (FE) models might address this issue by modelling precisely the machine geometry and components, for all physical phases of the simulation [4]. Yet for variable-speed/torque simulation purposes and for including system level simulation, FE models or co-simulation approaches cannot be considered for computational reasons. Thus, hybrid modelling frameworks can be envisaged [5]. These methods try to establish an efficient and reduced simulation approach by smartly combining the two previous ones. An example of such application is often referred to as look-up table approach. Offline simulations - electromagnetic, structural, acoustic - are performed and generate a component behavior depending on a set of inputs. Stored in tables, they are utilized in online system-level simulations where variable operating conditions are imposed. This type of approach allows to isolate computationally expensive tasks, to concentrate on fast operating condition simulation. Particularly regarding vibro-acoustic behavior, another approach is referred to as vibration synthesis, where instead of building tables, the FE model is reduced using a priori known generic force shapes. The method has gained interest over the last decade thanks to the exhaustive work of Boesing et al. [6], *e.g.* for combined experimental and numerical predictions [7], or as a quick alternative to standard FE methods reviewed in [8]. However consistent comparisons with FE methods in terms of accuracy against computational efforts is not documented to the authors knowledge.

In this paper, the efficiency of vibration synthesis methodology is evaluated. Section II lays the foundations to the multi-physical problem to solve, by introducing the standard FE technique and the vibration synthesis. Section III describes the application case which is a PMSM sized for an automotive vehicle and the offline simulation results. Finally Section IV confronts both methods in terms of accuracy of the simulated vibration and their associated computational efforts, to conclude on the vibration synthesis advantages and drawbacks.

II. Theoretical background

A. Standard modelling process

In a standard modelling process for vibration prediction, a magnetostatic time-stepping 2D FE analysis is performed for an operating point (torque T defined from a set of direct and quadrature currents (i_d,i_q), speed N) [8]. The resulted time-dependent magnetic field allows to calculate the magnetic force densities in the air-gap $\mathbf{F}_{|T,N}(t)$ using the Maxwell stress tensor [9]. They contain radial, tangential and axial

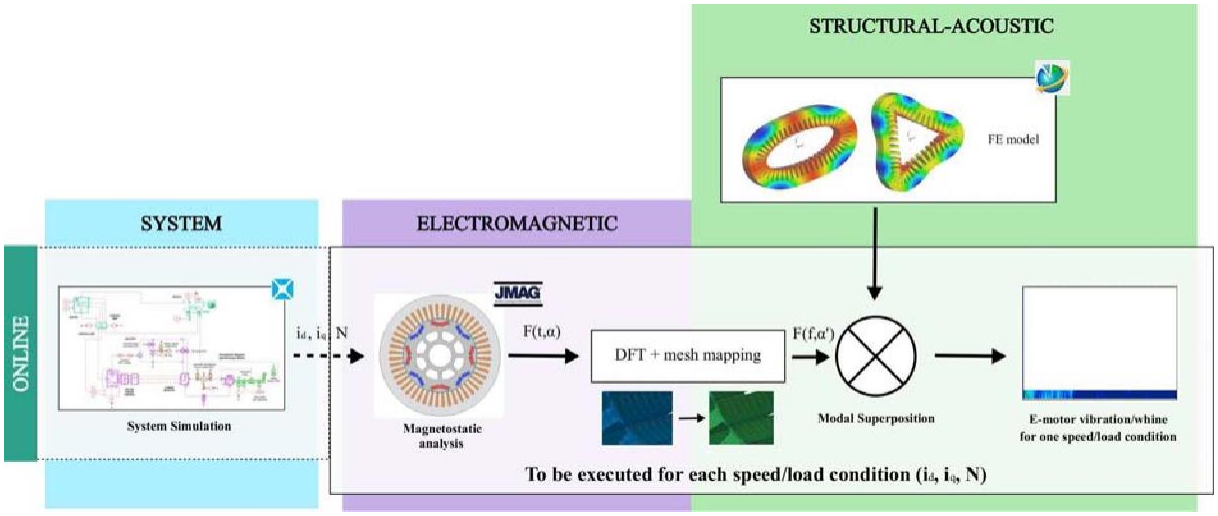

Fig. 1: Schematic of a standard multi-physical modelling process (one steady-state)

components; but only the radial components are taken into account here for the work purposes and because they are the largest contributors to vibrations [10]. Their Discrete Fourier Transforms (DFT) $\mathbf{F}|_{T,N}(f)$ are later applied to the structural system (3D FE model) via a conservative force mapping, and feed the equation of motion:

$$-4\pi^2 f^2\mathbf{M} + j2\pi f\mathbf{C} + \mathbf{K}\ \ \mathbf{X}(f) = \mathbf{H}(f)^{-1}\mathbf{X}(f) = \mathbf{F}|_{T,N}(f) \quad (1)$$

where **M**, **C** and **K** are the mass, damping and stiffness matrices, **X** the displacement field, and **H** the transfer function matrix. The size of each matrix is $(n_{DOF} \times n_{DOF})$ where n_{DOF} is the number of degrees-of-freedom (DOF) of the structural mesh. The forced vibration response in the frequency domain $\mathbf{X}(f)$ is then computed using the modal superposition technique [11].

Performing this analysis for every operating point along a torque and speed profile draws a colormap of the vibration outcome in operating conditions *i.e.* run-up, as shown in Fig. 1. It is important to note that the reconstructed run-up is thus assumed to be fully represented by a set of successive steady-state analyses, in turn neglecting all transient phenomena [12].

B. Vibration synthesis

Vibration synthesis works on the idea of performing simulations offline, *i.e.* in generic conditions, and online representing operating conditions. It essentially follows the flowchart of Fig. 2.

1) Of ine simulations: First following the hybrid approach described in [5], look-up tables are generated by performing several magnetostatic analyses for set currents i_d, i_q and rotor angular position ϑ; and storing the forces $\mathbf{F}(i_d, i_q, \vartheta)$. Ultimately the rotational speed N has only effects on the frequency signature of the magnetic field / force wave, *i.e.* no amplitude influences. This is easily understandable since the input to the full range of rotational speeds can be reconstructed by a single rotational speed simulation. Therefore for each operating point (T, N), the time t and space α dependent force wave $F(t,\alpha)|_{T,N}$ can be constructed.

Second, since this force wave has space and time distributions, it is possible to decompose it along 2 axis. Similarly as one decomposes a time signal in its Fourier series which harmonics are called frequencies, the force wave is also decomposed in a combination of force shapes F_m of spatial harmonic m, following the (cos,sin) orthogonal basis:

$$\begin{aligned} F(t,\alpha)|_{T,N} &= \sum_{m=-M}^{M} F_m(t,\alpha)|_{T,N} \\ &= F_0(t) + \sum_{m=1}^{M} F_{cos,m}(t)|_{T,N}\cos(m\alpha) \\ &\quad + \sum_{m=-M}^{-1} F_{sin,-m}(t)|_{T,N}\sin(-m\alpha) \end{aligned} \quad (2)$$

For vibration calculation purposes, the frequency domain complex forces $F_{cos,m}(f)|_{T,N}$ and $F_{sin,m}(f)|_{T,N}$ are used and correspond to the DFTs of the time-domain forces $F_{cos,m}(t)|_{T,N}$ and $F_{sin,m}(t)|_{T,N}$. It is important to note that M defines the number of spatial harmonics to consider and that the decomposition accounts for radial, tangential or axial components. As we work with FE models, M is logically limited by the number of nodes along the circumference of the EM mesh. For ease of illustration, Fig. 3 shows a snapshot (one time instant t) of the radial decomposition of a typical force wave at a particular operating point.

From this known decomposition, a reduced transfer scheme is defined on the structural level where instead of applying nodal forces in FE, a truncated group of force shapes (spatial harmonics) is applied. Offline, a set of unit forces $\mathbf{F}_{[r],m}$ with spatial order m is generated and mapped on the structural FE model. Their amplitude should be chosen such that the

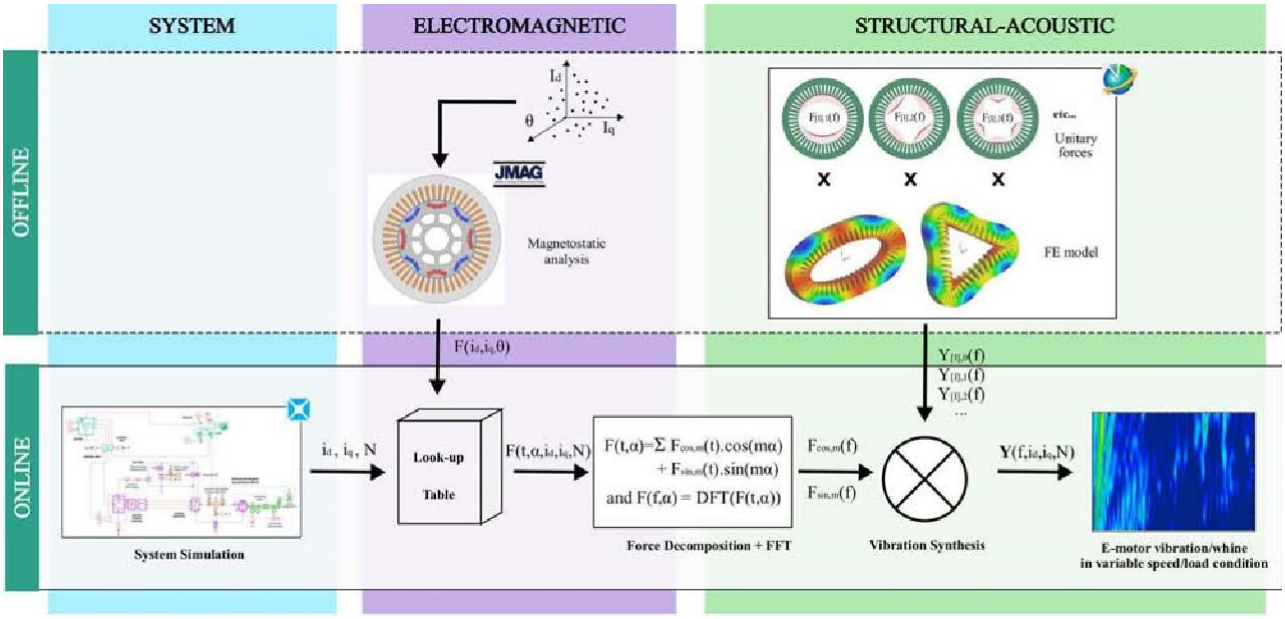

Fig. 2: Schematic of the vibration synthesis approach

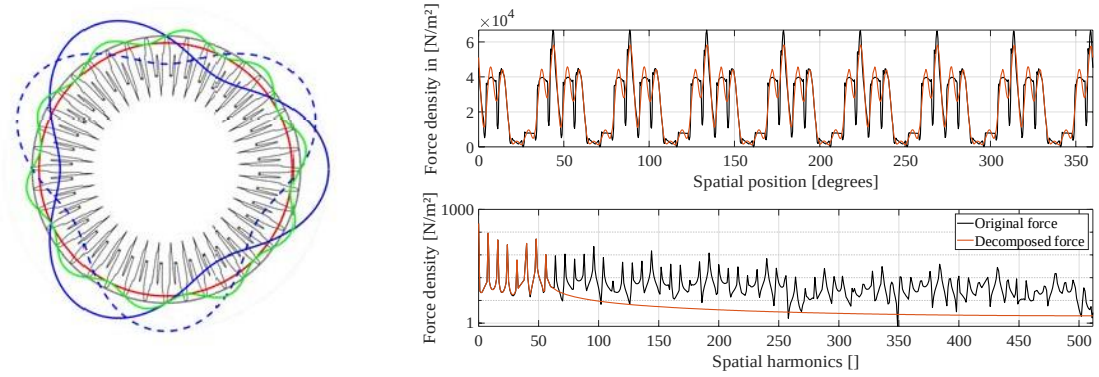

(a) Polar plot visualization, (black) Total radial force, (red) F_0, (blue) $F_{cos,3}$, (dashed blue) $F_{sin,3}$, (green) $F_{cos,10}$

(b) Snapshot of a radial force example and its decomposition up to 56 spatial harmonics

Fig. 3: Radial force decomposition examples

total energy per frequency line is equal to 1 N in order to ensure proper scaling on the later stages of the vibration synthesis. Ultimately a total of 2M+1 generic forces have to be created. The generic forces are then applied to the stator that transfers mechanical energy. By modal superposition principle, the generic complex vibration displacement $\mathbf{v}_{[r],m}$ is obtained,

$$\mathbf{v}_{[r],m}(f) = \mathbf{H}(f) \cdot \mathbf{F}_{cos,m}(f) \quad (3) \text{ where } m \in [-M, M]$$

2) Online simulations: First from an electromagnetic domain point of view, the operational magnetic forces from a system simulation that replicates steady-state condition, $F(t, \alpha)|_{T,N}$ are computed using the output $(i_d(t), i_q(t), \vartheta(t))$ and the offline generated look-up tables $\mathbf{F}(i_d, i_q, \vartheta)$. Second, these forces are decomposed following Eq. (2), and are used to scale the total vibration amplitude:

$$\begin{aligned}\mathbf{v}(f)|_{T,N} = {} & \underbrace{\mathbf{v}_{[r],0}(f) \cdot F_0(f)|_{T,N}}_{\mathbf{v}_0(f)|_{T,N}} \\ & + \sum_{m=1}^{M} \underbrace{\mathbf{v}_{[r],m}(f) \cdot F_{cos,m}(f)|_{T,N}}_{\mathbf{v}^{cos,m}(f)|_{T,N}} \\ & + \sum_{m=-M}^{-1} \underbrace{\mathbf{v}_{[r],m}(f) \cdot F_{sin,-m}(f)|_{T,N}}_{\mathbf{v}^{sin,-m}(f)|_{T,N}}\end{aligned} \quad (4)$$

Since the online simulations involve simple look-up tables

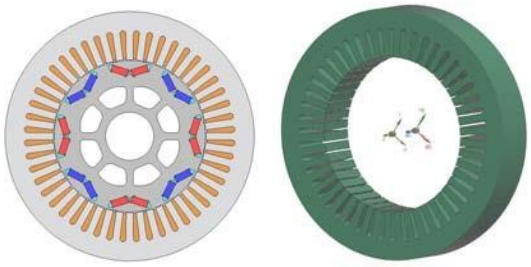

(a) Electromagnetic model in JMAG® (b) Structural mesh in Simcenter 3D®

Fig. 4: Electromagnetic and structural models

and variable multiplications, they do not require a lot of computational efforts. The burden is relocated to the offline simulations sides and the next Sections quantifies when and how much the vibration synthesis can benefit from standard processes.

III. Application to a PMSM

A. Machine specimen and simulation setup

The machine considered for the comparison of the two techniques is a 3-phase 48-slot-8-pole IPMSM. Table I describes several geometrical/performance characteristics, but more parameters can be found in the reverse-engineering study of [13].

TABLE I: Electric motor parameters

Parameter	unit	value
Peak power rating	kW	60
Peak torque	Nm	207
Base rotational speed	rpm	3,000
Stator outer diameter	mm	264
Stator stack length	mm	50.8
Air gap length	mm	0.73

Two-dimensional magnetostatic analyses are performed within JMAG® modelling software, and the corresponding model is pictured in Fig. 4a. Given the machine symmetries, only an eighth of the motor is modeled for computational time optimization. On the structural side, the three-dimensional model is created within Simcenter 3D® by considering the stator core to be the unique contributor to magnetically induced vibrations. Moreover linear isotropic behavior is used for the material properties of the laminations. These assumptions are commonly considered sufficient [3], [12], [14], and even more satisfactory in the context of comparing two modelling processes that use the same structural model. Yet the structural mesh was validated through convergence analysis of the natural frequencies and mode shapes. Fig. 4b illustrates the mesh generated for structural analyses.

B. Results

1) Electromagnetic simulation: In both modelling processes, the magnetic field needs to be calculated for a set of i_d and i_q currents. The resultant torque and radial force density are illustrated in Fig. 5 for i_d, i_q and N respectively set to 0 A, 60 A and 3,000 rpm, leading to an average torque of 47 Nm. It is important to remember that only radial components of the forces are considered in this paper, for both modelling processes.

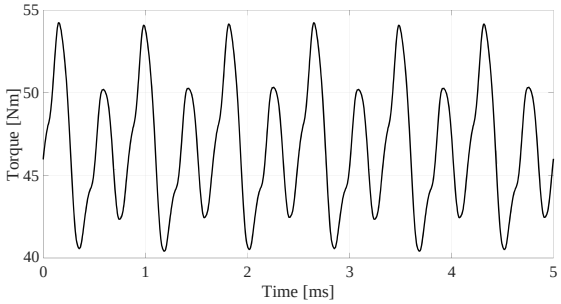

(a) Torque versus time at 3,000 rpm and $i_d = 0$ A, $i_q = 60$ A

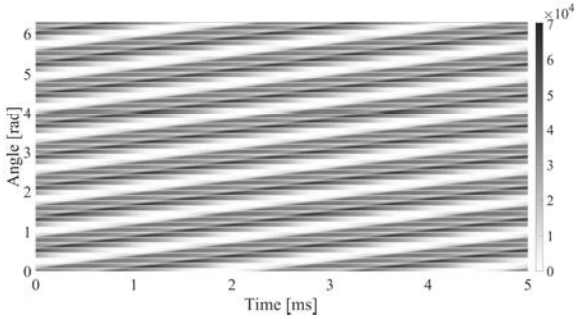

(b) Force density $F(t, \alpha)$ in N/m^2

Fig. 5: Torque and radial force density at 3,000 rpm and $i_d = 0$ A, $i_q = 60$ A

The force is clearly separated in 48 segments along the angle domain, which logically relates to the 48 slots of the machine. The DFT, through Fast Fourier Transform (FFT) algorithm, of the time-array signal permits to identify the frequency spectrum of the force wave and it is also common to calculate the DFT along the space-array. The combination of these two FFTs is often referred to as 2D FFT. Fig. 6 illustrates the 2D FFT graph obtained for the same operating point as represented previously.

First the frequency spectrum contains the fundamental electrical frequency multiplied by the number of rotor poles (*e.g.* 3,000/60×8 = 400 Hz at 3,000 rpm) with its harmonics (800 Hz, 1200 Hz, 1600 Hz, etc). Second along the space domain, the spatial harmonics directly relate to the force shapes illustrated in Fig. 3. This graphical representation of the force wave gives a large amount of information, since one can already detect a mode resonance excitation in the scenario where the force frequency and shape match the natural frequency and mode shape of the structure. Furthermore from this representation, it is possible to select a list of the most important force shape harmonics for the vibration synthesis. To this end, the summation of the force density per shape

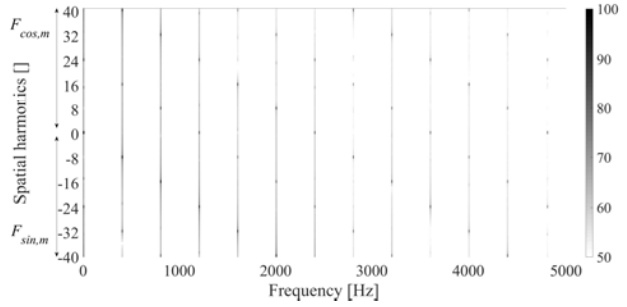

Fig. 6: Force density $F_{cos/sin,m}(f)$ in dB(Ref.1e-6 N/m^2) at 3,000 rpm and i_d = 0 A, i_q = 60 A

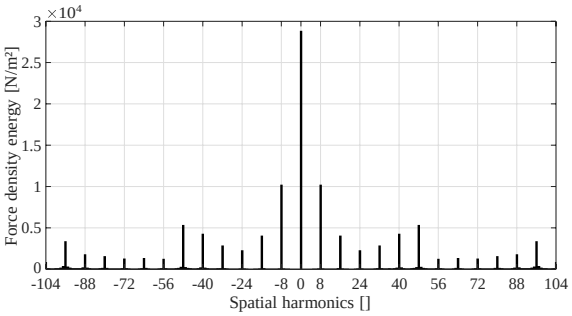

Fig. 7: Force density energy at 3,000 rpm and i_d = 0 A, i_q = 60 A

harmonics along the frequency axis is calculated. It represents the total force energy per shape harmonics and is shown in Fig. 7 for the studied machine. Shapes harmonics 0, 8, 48, 40, 16, 96 and 24 (with their negative) are the largest contributors to the total force, in order of importance. They are taken into account in the next vibration synthesis calculations.

2) Structural simulation: The modal analysis performed during both modelling approaches provides the structural intrinsic behavior of the machine. Table II shows the resulted natural frequencies up to 5,000 Hz. The mode shapes are categorized following their (a,b) values, where a represents half the number of nodal lines (zero radial displacement) along the stator circumference and b the number of nodal lines along the shaft axis. (2 axial) mode is a particular shape where axial deformations occur. It is important to note that the number a (and its twin mode) is intimately linked to the force spatial harmonic m (positive and negative) [15] as they correspond to the same radial distribution.

TABLE II: Modal analysis results - all modes have a twin shifted of 45 degrees

Mode	Frequency [Hz]	Mode	Frequency [Hz]
(2,0)	642	(3,1)	3639
(2,1)	1310	(5,0)	4084
(3,0)	1685	(6,0)	4914
(4,0)	2922	(0,0)	4934
(2 axial)	3479		

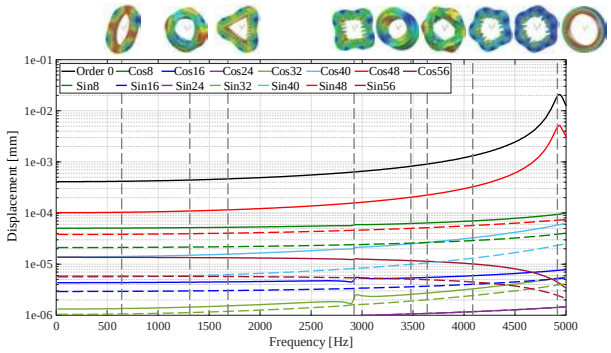

Fig. 8: Generic vibration displacements $\mathbf{v}_{[r],m}$ with mode shapes at their natural frequency

As explained in Section II-B1, generic vibration displacements are computed for shape orders 0, 8, 48, 40, 16, 96 and 24 (with their negative). Fig. 8 shows the corresponding generic vibration displacements, and particularly highlights the high contribution of force shapes 0 and 48 on the structure. In fact the mode (0,0) is the only mode excited by the force shapes taken into account, within the frequency range from 0 to 5,000 Hz.

IV. Comparisons and Discussions

1) Accuracy: In terms of accuracy, the two modelling approaches are compared for 8 different rotational speeds ranging from 500 rpm to 5,000 rpm, and fixed (i_d,i_q) to (0 A, 60 A). As seen in Fig. 9, the vibration displacement levels stand within similar order of magnitudes, and high amplitude order lines (multiples of 8) occur. The standard process yet contains additional frequency lines which might indicate a lack of spatial harmonic content in the decomposed force used in vibration synthesis. Nevertheless former studies show the sufficiency of considering uniquely lower orders [6], [15], in comparison with experiments, which questions the reliability of the standard process.

Besides this questioning, it is necessary to define a protocol to define the optimum number of spatial harmonics to be considered in the vibration synthesis. As suggested in this paper, a list of the most important spatial harmonics based on the total energy contribution can be extracted. Fig. 10 presents the vibration displacement for 3 different lists of harmonics – negative harmonics are used as well in the calculations. Significant discrepancies are observable for some orders, notably 16, 32, 40 and 48, with up to 4 dB deviations. Logically, the higher the number of harmonics considered, the higher the vibration output. These two remarks give an explanation to the non-perfectly-correlated results of Fig. 9, emphasized by the fact that at most 7 harmonics out of a total of 120 (negative excluded) are taken into account here.

2) Computational effort: On another side, computational efforts are significantly different from one modelling approach to another. Hence the computational times were estimated based on several simulations time gathered for each approach

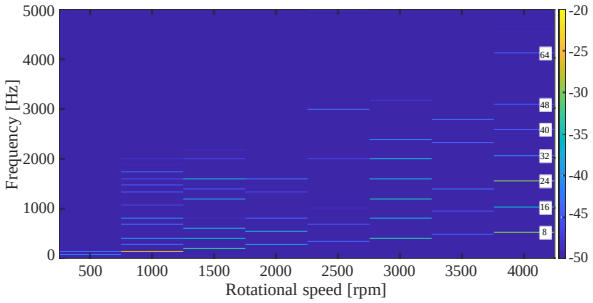

(a) Standard process

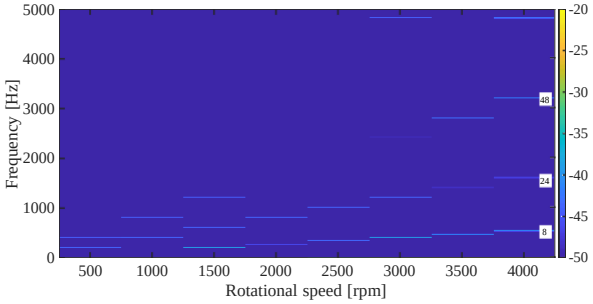

(b) Vibration synthesis

Fig. 9: Vibration displacement output (in dB) for different modelling processes

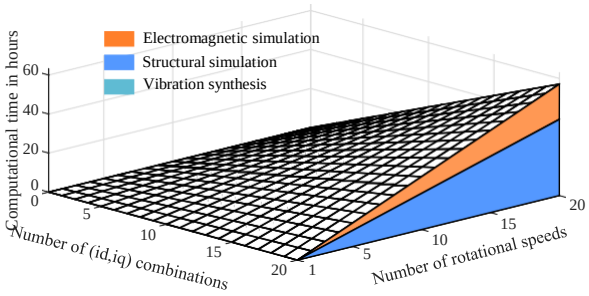

(a) Standard process

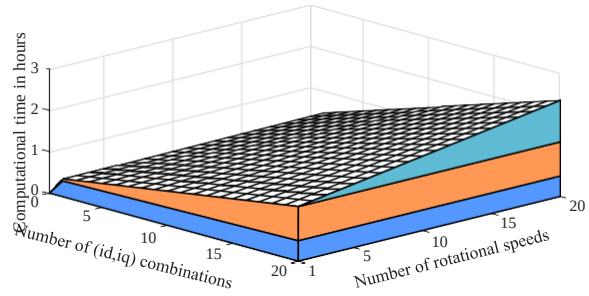

(b) Vibration synthesis

Fig. 11: Computational efforts depending on the number of operating points simulated

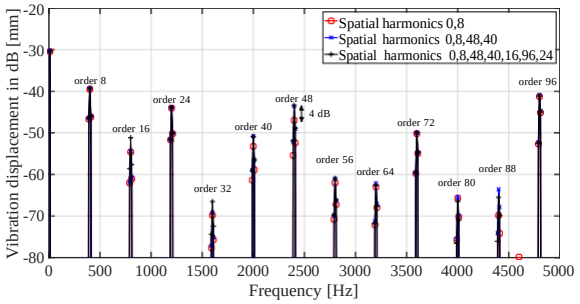

Fig. 10: Vibration displacement output for different spatial harmonics lists, at 3,000 rpm and $i_d = 0$ A, $i_q = 60$ A

and averaged, and shown in Fig. 11. The same computer was used during the simulations, *i.e.* a Dell Precision 7520 with Intel(R) Core(TM) i7-7920HQ CPU (3.10 GHz) and 32 Gb of RAM memory. One electromagnetic and one structural simulation approximately takes 0.05 and 0.025 hour respectively. During offline simulations, 15 shapes were considered for the generic transfer functions calculations and the rotational speed variation could be disregarded for the vibration synthesis as explained in Section II-B1. For the standard process, the total required time linearly depends on the number of operating points (T ,N) which discredits its use when a large amount of operating points have to be calculated. On the contrary, the vibration synthesis front-loads the large computational effort within the offline simulation step, while the online simulations can be very fast; *e.g.* approximately 30 times faster for 20×20 operating points.

Finer speed discretization of the vibration results can be obtained with vibration synthesis, yet quickly. For example, Fig. 12 represents a run-up simulation at 47 Nm where clear orders and resonance lines can be identified. It is important to note that this process also permits to weight force shape contributions by simple colormap extraction, see Fig. 12 and 13. Here shape 0 is largely contributing to the total response for orders multiples of 48, while shape 8 has a major contribution towards order 8. This enables more detailed troubleshooting and target setting towards vibration mitigation.

V. Conclusions

In this paper, the vibration synthesis was confronted to the standard FE process for the vibration prediction of electric machines. While the standard process involves computations for each particular operating point, the vibration synthesis uses offline and online simulations to ease the calculations. This implies significant computational time improvements, which was shown for an automotive-sized machine to reach a factor 30 for run-up analyses. However accuracy is affected and essentially comes from the force shape truncation involved in the vibration synthesis. A selection protocol, based on an energy contribution analysis, was therefore proposed and provides quantitative measures to the effects on the vibration levels. Next, it would be important to correlate both methods against experiments as it was noticed that the standard process does not reflect with the common literature conclusions about several orders present in the spectra. Ultimately, the work can

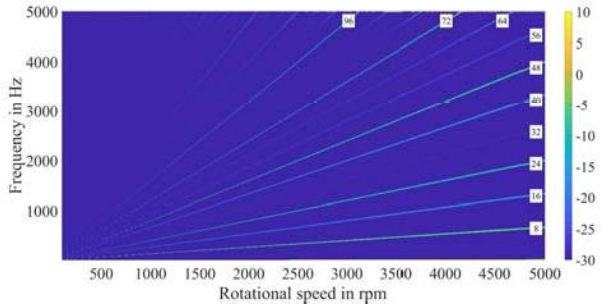

(a) Total contribution - $v(f)$

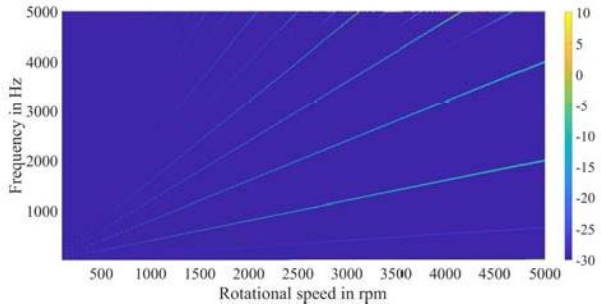

(b) Contribution from shape 0 - $v_0(f)$

Fig. 12: Vibration displacement output (in dB) using the vibration synthesis

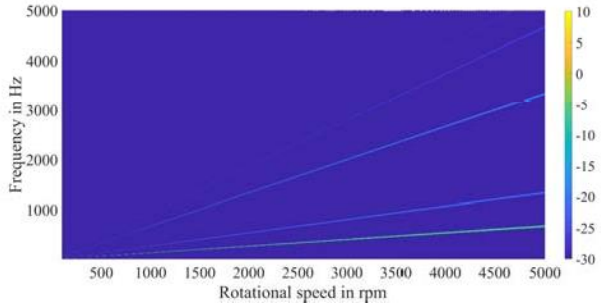

(a) Contribution from shape 8 (cos) - $v_{cos,8}(f)$

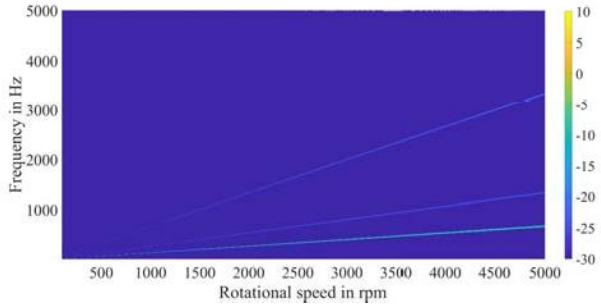

(b) Contribution from shape 8 (sin) - $v_{sin,8}(f)$

Fig. 13: Vibration displacement output (in dB) using the vibration synthesis

be extended to acoustics as it would bring an extra physical layer to the problem.

ACKNOWLEDGMENT

This paper is part of the European Industrial Doctorate on Next Generation for Sustainable Automotive Electrical Actuation project (INTERACT) which is a European Union Horizon 2020 research and innovation programme, grant number 766180. The authors also would like to acknowledge JSOL Corporation for granting access to JMAG® software packages.

REFERENCES

[1] A. Stefanskyi, A. Dziechciarz, F. Chauvicourt, G. Sfakianakis, K. Ramakrishnan, K. Niyomsatian, M. Curti, N. Djukic, P. Romanazzi, S. Ayat, S. Wiedemann, W. Peng, S. Stipetic, and A. Tamas, "Researchers within the EU funded Marie Curie ITN project ADEPT, grant number 607361," 2013.

[2] J. F. Gieras, C. Wang, and J. C. Lai, *Noise of polyphase electric motors*, ser. Electrical and computer engineering. Boca Raton, Fla.: CRC/Taylor & Francis, 2006, no. 129.

[3] J. Le Besnerais, "Réduction du bruit audible d origine magnétique dans les machines asynchrones alimentées par MLI - regles de conception silencieuse et optimisation multi-objectif," Ph.D. dissertation, Ecole Centrale de Lille, 2008.

[4] J. B. Dupont and P. Bouvet, "Noise radiated by an electrical powertrain: multiphysical simulation," 2013. [Online]. Available: http://documents.irevues.inist.fr/bitstream/handle/2042/52154/a_1KJK8L72.pdf?sequence=1&isAllowed=y

[5] F. L. M. dos Santos, J. Anthonis, F. Naclerio, J. J. C. Gyselinck, H. Van der Auweraer, and L. C. S. Goes, "Multiphysics NVH Modeling: Simulation of a Switched Reluctance Motor for an Electric Vehicle," *IEEE Transactions on Industrial Electronics*, vol. 61, no. 1, pp. 469–476, Jan. 2014. [Online]. Available: http://ieeexplore.ieee.org/lpdocs/epic03/wrapper.htm?arnumber=6461408

[6] M. Boesing, "Acoustic modeling of electrical drives: noise and vibration synthesis based on force response superposition," Ph.D. dissertation, RWTH Aaachen university, Aachen, 2014.

[7] A. Saito, M. Kuroishi, and H. Nakai, "Empirical Vibration Synthesis Method for Electric Machines by Transfer Functions and Electromagnetic Analysis," *IEEE Transactions on Energy Conversion*, vol. 31, no. 4, pp. 1601–1609, Dec. 2016. [Online]. Available: http://ieeexplore.ieee.org/document/7466837/

[8] J. Le Besnerais, "Fast prediction of variable-speed acoustic noise due to magnetic forces in electrical machines," 09 2016, pp. 2259–2265.

[9] R. Pile, G. Parent, E. Devillers, T. Henneron, Y. Le Menach, J. Le Besnerais, and J. Lecointre, "Application limits of the airgap maxwell tensor," in *IEEE Conference on Electromagnetic Field Computation (CEFC)*, 2018.

[10] E. Devillers, M. Hecquet, J. Le Besnerais, and M. Rgniez, "Tangential effects on magnetic vibrations and acoustic noise of induction machines using subdomain method and electromagnetic vibration synthesis," in *Electric Machines and Drives Conference (IEMDC),*

2017 IEEE International. IEEE, 2017, pp. 1–8. [Online]. Available: http://ieeexplore.ieee.org/abstract/document/8002072/

[11] D. J. Inman, *Engineering Vibration*, 4th ed. Pearson Education, Inc., 2014.

[12] F. Chauvicourt, "Vibro-acoustics of rotating electric machines: Prediction, validation and solution," Ph.D. dissertation, Katholieke Universiteit Leuven and Université Libre de Bruxelles, 2018.

[13] T. J. E. Hendershot, "MotorSolve analysis of the 2010 Toyota Prius Traction Motor," in *Infolytica engage user conference*, Chicago, 2015.

[14] J. R. Hendershot, "Causes & Sources of audible noise in elecric motors," in *22nd Incremental Motion Control Systems and Devices Symposium*. Champaign IL: B.C. Kuo Ed., 1993, pp. 259–270.

[15] P. Kotter, W. Bischof, R. Kennel, O. Zirn, and K. Wegener, "Noise-vibration-harshness-modeling and analysis of induction drives in E-mobility applications," in *2017 IEEE International Electric Machines and Drives Conference (IEMDC)*. Miami, FL, USA: IEEE, May 2017, pp. 1–8. [Online]. Available: http://ieeexplore.ieee.org/document/8002148/